catalysts

MDPI

Article

Application of Floating TiO_2 Photocatalyst for Methylene Blue Decomposition and *Salmonella typhimurium* Inactivation

Marius Urbonavicius [1], Sarunas Varnagiris [1,*], Sandra Sakalauskaite [2], Emilija Demikyte [2], Simona Tuckute [1] and Martynas Lelis [1]

[1] Center for Hydrogen Energy Technologies, Lithuanian Energy Institute, 3 Breslaujos, 44403 Kaunas, Lithuania; marius.urbonavicius@lei.lt (M.U.); simona.tuckute@lei.lt (S.T.); martynas.lelis@lei.lt (M.L.)

[2] Department of Biochemistry, Faculty of Natural Sciences, Vytautas Magnus University, 44403 Kaunas, Lithuania; sandra.sakalauskaite@vdu.lt (S.S.); emilija.demikyte@vdu.lt (E.D.)

* Correspondence: sarunas.varnagiris@lei.lt; Tel.: +370-37-401-824

Abstract: The growing level of wastewater as well as pollution of freshwater by various bacteria are essential worldwide issues which have to be solved. In this contribution, nanocrystalline anatase TiO_2 films deposited by magnetron sputtering on high-density polystyrene (HDPE) beads were applied as floating photocatalysts for *Salmonella typhimurium* bacterial inactivation in water for the first time. Additionally, the photocatalytic degradation of methylene blue dye in the presence of HDPE beads with TiO_2 film under UV-B irradiation was investigated. The suitability to adopt such floating photocatalyst structures for practical applications was tested in cycling experiments. The detailed surface morphology, crystal structure, elemental mapping, surface chemical composition and bond analysis of deposited TiO_2 films were investigated by scanning electron microscope, X-ray diffractometer and X-ray photoelectron spectroscope techniques. The bacterial viability as well as MB decomposition experiments showed promising results by demonstrating that 6% of bacterial colonies were formed after the first run and only about 1% after the next four runs, which is an appropriate outcome for practical applications. NPN uptake results showed that the permeability of the outer membrane was significantly increased as well.

Keywords: floating photocatalyst; anatase TiO_2; thin films; magnetron sputtering; *Salmonella typhimurium*

Citation: Urbonavicius, M.; Varnagiris, S.; Sakalauskaite, S.; Demikyte, E.; Tuckute, S.; Lelis, M. Application of Floating TiO_2 Photocatalyst for Methylene Blue Decomposition and *Salmonella typhimurium* Inactivation. *Catalysts* **2021**, *11*, 794. https://doi.org/10.3390/catal11070794

Academic Editor: Vincenzo Vaiano

Received: 15 June 2021
Accepted: 27 June 2021
Published: 29 June 2021

1. Introduction

The main purpose of any type of catalyst is to decrease the activation energy of the desired chemical reaction and to promote the formation of favored reaction products. Stimulated by process optimization and cost reduction trends, catalysis has become one of the most important fields in industry and chemistry, and currently up to 85–90% of industrial processes include at least one catalytic step [1]. Recently, catalytic processes have started to be implemented in even more areas outside industrial production and they have become an important part of sustainable environmental care technologies as well [2–7].

One of the most well-known environmental issues is the increasing demand for freshwater sources for human consumption. The limited availability of clean drinking and surface water has become a worldwide problem owing to the occurrence and spread of pathogenic bacteria, such as *Escherichia coli* (*E. coli*), *Salmonella* spp., etc. These types of bacteria have been frequently detected in wastewater treatment plants (WWTPs) and without appropriate treatment they can spread and infect drinking or surface water reservoirs and cause harm to human health [8,9]. For example, *Salmonella* is a facultative anaerobic Gram-negative rod-shaped bacillus considered the predominant pathogenic bacterium in wastewater. The majority of its species are harmful to humans and cause various illness such as gastroenteritis, abdominal discomfort, diarrhea and vomiting in hosts [10].

The illnesses caused by *Salmonella* are closely related to the fact that conventional wastewater treatment does not guarantee elimination of all pathogens and resistance in bacteria. Some studies showed that *Salmonella* have been frequently found in WWTPs in either influents and effluents even after the disinfection process [9,11]. Furthermore, a study presented by Dolejska et al. revealed that general WWTP conditions suggest suitable ecosystems for the transfer, evolution and spread of resistance genes as well as close contact of bacteria [12]. Such bacteria and resistance genes might be disseminated via surface water structures [13]. Therefore, the development of alternative wastewater treatment, especially bacteria disinfection technologies, is highly required in order to successfully combat consequences of bacterial spread.

Recently, advanced oxidation processes (AOPs) have been attracting a lot of attention due to AOPs' versatility for the inactivation of various bacteria [14], viruses [15], fungi [16], etc., as well as the possibility to apply these technologies for both air purification [17] and/or wastewater cleaning [18]. Generally, AOPs involve the formation of highly reactive oxygen species (ROS), for instance, hydrogen peroxide (H_2O_2), superoxide radicals ($O_2^{\bullet -}$), hydroxide radicals ($OH^{\bullet}$), etc., which act as an oxidizing agents and cause damage to the membranes, proteins, enzymes, DNA and RNA of pathogenic microorganisms [19,20].

The usage of specific semiconductive oxide catalysts (for example, TiO_2 [5] or ZnO [21]) and initiation of the photocatalytic generation of ROS species is one of the most promising AOP branches. However, in real-world conditions, photocatalytic water disinfection often faces practical challenges because it requires photoactive materials, which most often are powders or thin films deposited on various substrates. The application of photoactive powders for wastewater cleaning is complex because of their inconvenient separation from water after the treatment process. Meanwhile, thin films synthesized on traditional substrates, like glass, sink and therefore suffer a lack of the light irradiation necessary for the photocatalysis process. The issue related to the low light capture efficiency is common to all photocatalysts that sink in water. Additionally, thin films are usually characterized by relatively low surface area and reduced photocatalytic efficiency compared to powders [22–24].

During the last decade, the new concept of a "floating photocatalyst" [22,23] was recognized as potentially better solution in comparison to the traditional photocatalyst forms (i.e., free powders or coatings on sinking substrates). Floating photocatalysts ensure the highest possible light adsorption, which reduces the energy loss when compared with "underwater" photocatalysts, and increase the pollutant decomposition efficiency. High oxygenation of the photocatalyst is ensured due to the proximity to the air/water interface. Additionally, in many cases, floating photocatalyst systems can be installed without a complicated operation system and the loss of photocatalysts during water treatment or separation is minimized [22]. Unfortunately, there is still a lack of scientific and technical knowledge about photocatalysts immobilized onto various floating substrates and their application in bacterial inactivation or other real pollutant (fungi, pharmaceuticals, etc.) disinfection experiments. In fact, there have been various studies aimed at organic contaminant decomposition (i.e., Rhodamine B, methylene blue, etc.) [22,23,25,26], but only a few focused on bacterial inactivation [27–29].

In the current work, anatase phase TiO_2 films were deposited by the magnetron sputtering (MS) technique on floatable high-density polyethylene (HDPE) beads. Both the MS TiO_2 synthesis method and the choice of HDPE for the substrate have some beneficial properties. For example, in general, MS is a one-step process which allows the deposition of anatase phase TiO_2 films under room temperature conditions, whereas floatable HDPE substrate beads are inexpensive, durable, do not degrade in water and can be easily extracted from aqueous solutions and recycled (as well as produced from other recycled HDPE products). Nevertheless, the MS method and HDPE beads are rarely used by researchers [22,23] and we do not know of any study in which they have been used in combination. The efficiency of floating TiO_2-based photocatalysts on HDPE beads was tested with *Salmonella typhimurium* bacterial inactivation and compared to methylene blue

dye bleaching under UV-B light irradiation. In this way, we filled the knowledge gap of the application of a floating photocatalyst to one bacterium that is most widespread and harmful to human health—*Salmonella typhimurium*. Cycling experiments were performed to check the durability of the TiO_2 photocatalyst–floating substrate system as well. The precise analysis, including structure, morphology, elemental composition and chemical bonds, was accomplished before and after dye and bacterial decomposition experiments.

2. Results

The XRD pattern of TiO_2 film deposited on HDPE beads is presented in Figure 1. The observed diffraction pattern corresponds to a crystalline anatase structure (tetragonal, I41/amd) with three characteristic peaks at 25.3°, 48.1° and 55.1°, which can be assigned to the (101), (200) and (211) diffraction planes of anatase TiO_2, respectively. It is worth noting that we did not find any other peaks, otherwise it is typical for characteristic anatase. The average crystallite size was estimated to be 33.2 nm (R_{wp} = 1.733), therefore showing the nanocrystalline nature of deposited TiO_2 films.

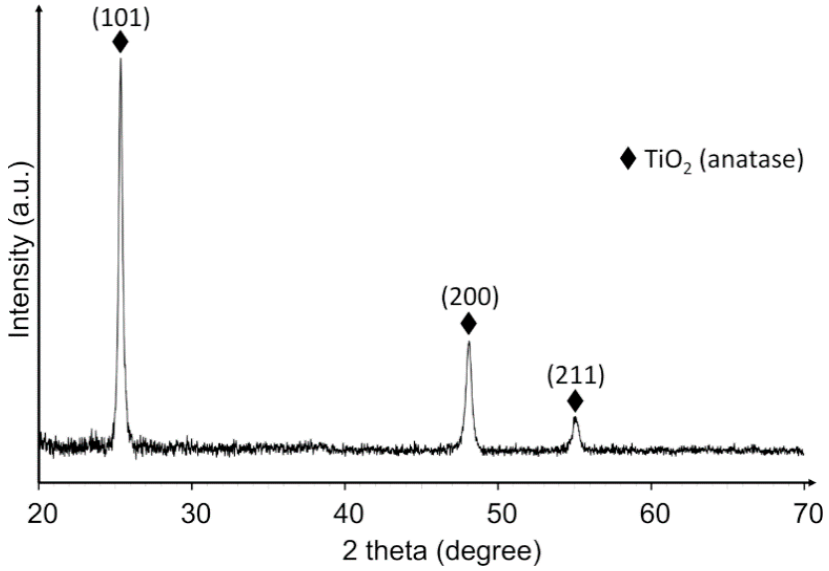

Figure 1. XRD pattern of TiO_2 film deposited on the surface of HDPE beads.

It is known that sputtering power and deposition time have great influence on the formation of the crystal structure and intensity of diffraction peaks [30]. Moreover, polycrystal anatase can be influenced by factors such as film thickness, working gas pressure, oxygen partial pressure and substrate temperature [31]. This means that more pronounced crystallographic orientations of anatase can be obtained with the increase in sputtering power density [32]. However, in our case, the temperature could also increase which would lead to the destruction of HDPE beads. Therefore, mild magnetron sputtering conditions were preselected.

Figure 2a,b present SEM images and elemental mapping results of HDPE beads without and with deposited TiO_2 film on their surface. Firstly, elemental mapping confirmed the relatively uniform distribution of Ti and O elements over the whole area of HDPE beads after the TiO_2 deposition process (Figure 2b). Still, some small cracks or the absence of TiO_2 film may be observed which were presumably caused by friction between beads during their storage (Figure 2b).

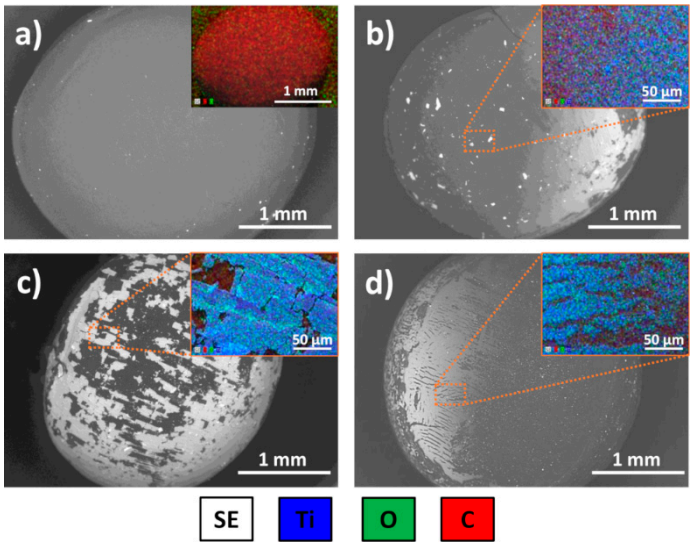

Figure 2. SEM view images and elemental mapping results: (**a**) primary HDPE bead; (**b**) HDPE + TiO_2; (**c**) HDPE + TiO_2 after 5th run of MB decomposition; (**d**) HDPE + TiO_2 after 5th run of *Salmonella typhimurium* SL1344 bacterial inactivation.

The significant surface alteration of HDPE beads with TiO_2 film was observed after their utilization for five cycles of MB decomposition or bacterial inactivation experiments. The results revealed much larger areas with detached TiO_2 films in both cases (Figure 2c,d). However, this is quite predictable, as beads have to undergo several stages where TiO_2 can be detached, such as: storage, where beads are rubbing against each other; MB decomposition or bacterial inactivation experiments, where rotation with 500 rpm is used; washing with water after every cycle. Despite that, the majority of HDPE beads were still covered with TiO_2 film even after five cycles. This result shows the good adhesion characteristics between the deposited TiO_2 and HDPE surface, which are directly related to the effective application of such beads for repeated usage as a photocatalyst. (see further cycling results below).

Figure 3a demonstrates the decrease in the characteristic absorbance band, at 664 nm, of MB dye during its decomposition using HDPE covered by TiO_2 film under UV-B irradiation for 180 min. A continuous decreasing trend from 1.35 down to 0.11 within 3 h was observed in the absorption peak value (almost 92% of MB dye was degraded). On the other hand, Figure 3b illustrates the plot of C/C_0 versus irradiation time where C and C_0 are residual and initial concentrations of MB and the C/C_0 ratio decreased by more than 80% in 180 min (from 1 down to 0.18).

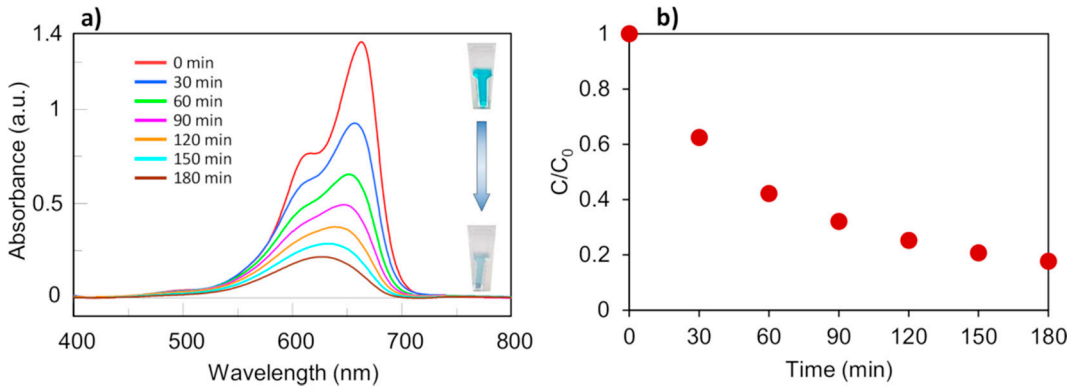

Figure 3. (**a**) UV–visible absorbance spectra indicating the photocatalytic degradation of MB dye using HDPE-TiO_2 under UV-B irradiation and (**b**) plot of C/C_0 versus time under UV-B irradiation.

The photocatalytic properties of the HDPE beads coated by TiO_2 were assessed via an MB degradation test. Cycling experiments were repeated using the same sample in the following runs (Figure 4a). The reaction rate constants were calculated from the slopes of ln(C/Co) versus time plots and are presented in Figure 4b. Before the experiment, the influence of UV-B-induced photolysis (without photocatalyst) and adsorption of MB into the surface of the samples were estimated. The direct photolysis effect was evaluated by degradation of MB without photocatalytic material under the same irradiation of UV-B and other conditions as used for samples with TiO_2 film (see Methodology). Meanwhile, the adsorption effect was investigated when HDPE beads with TiO_2 film were immersed in the MB solution for 180 min without any light irradiation (measured every 30 min). However, the photolysis and adsorption factors were negligible, with k values of 0.3×10^{-3} and 0.2×10^{-3} min^{-1}, respectively.

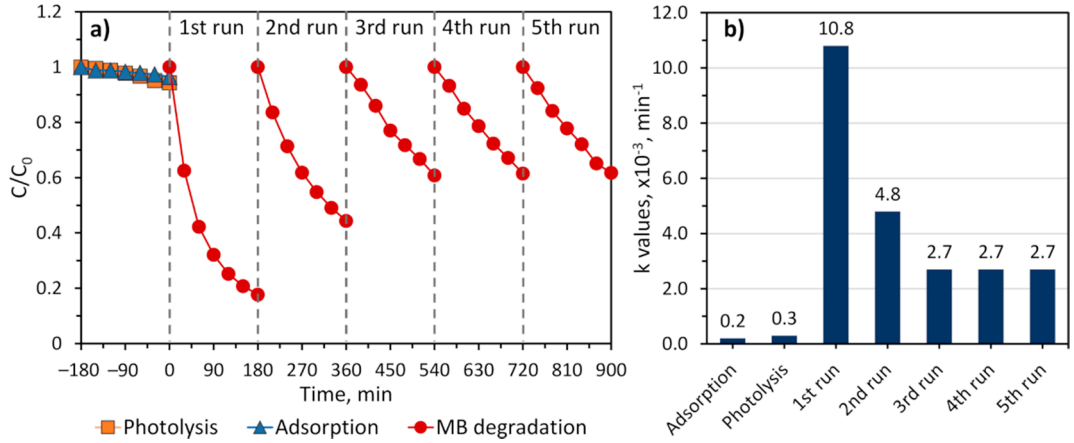

Figure 4. (**a**) Effect of cycling runs on photocatalytic degradation of MB dye in the presence of HDPE-TiO_2 under UV-B irradiation and (**b**) rate constants of photocatalytic degradation.

The highest MB degradation rate was observed after the 1st run of photocatalytic testing (k value 10.8×10^{-3} min^{-1}), while it decreased more than two times after the 2nd run (k value 4.8×10^{-3} min^{-1}). After the 3rd run, it decreased less than twice (k value 2.7×10^{-3} min^{-1}) and then remained stable during the 4th and 5th runs. The decreased degradation rate could be caused by the TiO_2 loss when beads were rubbing against each other during mixing as well as the recovery procedure after the photocatalytic run was finished. It is likely that, during the first runs, some weakly adhered TiO_2 film was peeled off the surface of HDPE. This may be related to the protrusions and bumps of the HDPE surface which rubbed against each other the most during the stirring. Meanwhile, in run 3 and subsequent runs, the most strongly adhered HDPE remained unchanged (particularly film in depressions of the surface). Despite the very low adsorption rate, a bluish surface of HDPE beads with TiO_2 was observed. Sedimentation of MB dye around the photocatalyst after each run of photocatalytic degradation still took place and might have led to the decrease in the degradation rate. This is in agreement with the XPS results presented in Figure 5.

The degradation rate was still significant even after still photocatalytic cycles, which shows a promising photocatalytic performance for applications in water treatment photocatalysis. If the assumption of the predominant role of the physical peeling of active TiO_2 film is true, the issue of low adhesion between HDPE beads and TiO_2 film could potentially be solved by one of the traditional measures: (i) usage of primers [33]; (ii) polymer surface pretreatment by plasma and/or other technologies [34–38]. On the other hand, advanced floating polymer structures (such as specially designed floating media widely used for the moving bed biofilm reactors [39–41]) could provide a large fraction of active surface area which is completely protected from mechanical brushing or scratching by polymer collisions.

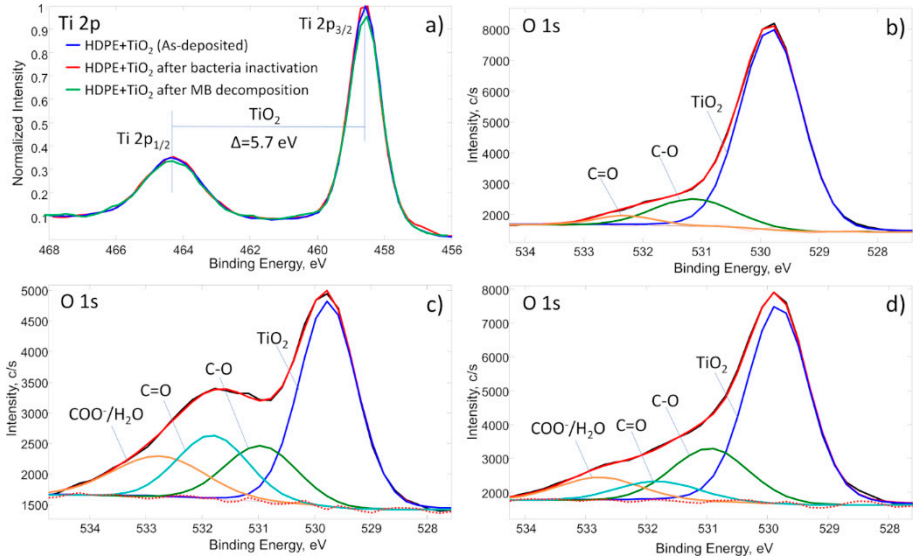

Figure 5. XPS deconvolution spectra: (**a**) Ti 2p spectra at normalized intensity including as-deposited HDPE + TiO_2 (blue line), HDPE + TiO_2 after bacterial inactivation (red line) and HDPE+TiO_2 after MB decomposition (green line); (**b**) O 1s spectra of as-deposited HDPE + TiO_2; (**c**) O 1s spectra of HDPE + TiO_2 after MB decomposition; (**d**) O 1s spectra of HDPE + TiO_2 after bacterial inactivation.

The XPS technique was used for surface elemental and chemical bond analysis of TiO_2 films deposited on the HDPE substrates before and after MB decomposition and *Salmonella typhimurium* bacterial inactivation experiments. The elemental analysis revealed the existence of C, O and Ti after TiO_2 synthesis on the HDPE substrate by confirming that any unwanted impurities were not immobilized during the magnetron sputtering process (Table 1). The results of chemical bond analysis are shown as the high-resolution spectra of Ti 2p and O 1s in Figure 5a–d. Figure 5a represents Ti 2p spectra at three different states of samples: as-deposited, after bacterial inactivation and after MB decomposition experiments. As can be seen, all three spectra have identical shapes with the same binding energies at the top of the peaks (i.e., 458.6 eV and 464.3 eV). The fitting results, as well as the difference between the two mentioned peaks (Δ = 5.7 eV), confirms the formation of pure TiO_2 phase, which remained stable even after bacterial inactivation or MB decomposition experiments. Nevertheless, the results of elemental composition suggest that the amount of Ti and O decreased after both experiments. Moreover, additional elements were detected, including N (1.9 atom.%) after MB decomposition and N (2.3 atom.%), P (1.0 atom.%) and Ca (0.7 atom.%) after bacterial inactivation experiments. These findings describe the adsorption process of decomposed materials (MB or *Salmonella typhimurium*), and that N is an ingredient of MB and N, P and Ca were adsorbed from *Salmonella typhimurium* bacterial medium. Additionally, the amount of C increased after both experiments, from 32.7 atom.% in as-deposited samples to 56.8 and 39.1 atom.% in samples after MB decomposition or bacterial inactivation, respectively. This alteration is directly related to the increased amount of various carboxyl groups, including C–O (530.9 eV), C=O (531.8 eV) and COO^- (532.8 eV) after decomposition of both water pollutants. Specifically, deconvolution of the O 1s peak revealed the increment in the area ratio between carboxyl groups and TiO_2 (carboxyl/TiO_2 in area%) from 0.21 in as-deposited samples to 0.95 and 0.61 in samples after MB decomposition or bacterial inactivation, respectively. It shows that the largest amount of carboxyl group compounds was formed on samples used for MB decomposition. This finding supports the MB decomposition cycling results, which suggest that the decomposition ratio (k value) decreased after first two runs, and then remained relatively stable during all further runs (Figure 4), while cycling of *Salmonella typhimurium* inactivation experiments showed a similar inactivation rate during all runs (Figure 6). Therefore, we speculate that this alteration of the MB decomposition rate during the cycling

process is related to the combination of bead deterioration due to friction processes and higher adsorption (compared to cycling of bacterial inactivation, see Figures 5d and 6a) of carboxyl groups on the bead surface during decomposition experiments.

Table 1. XPS surface elemental composition, atom%.

Sample	C	O	Ti	N	P	Ca
HDPE	92.9	7.1	-	-	-	-
HDPE + TiO_2	32.7	48.4	18.9	-	-	-
HDPE + TiO_2 after MB decomposition	56.8	33.1	8.2	1.9	-	-
HDPE + TiO_2 after bacterial inactivation	39.1	44.6	12.3	2.3	1.0	0.7

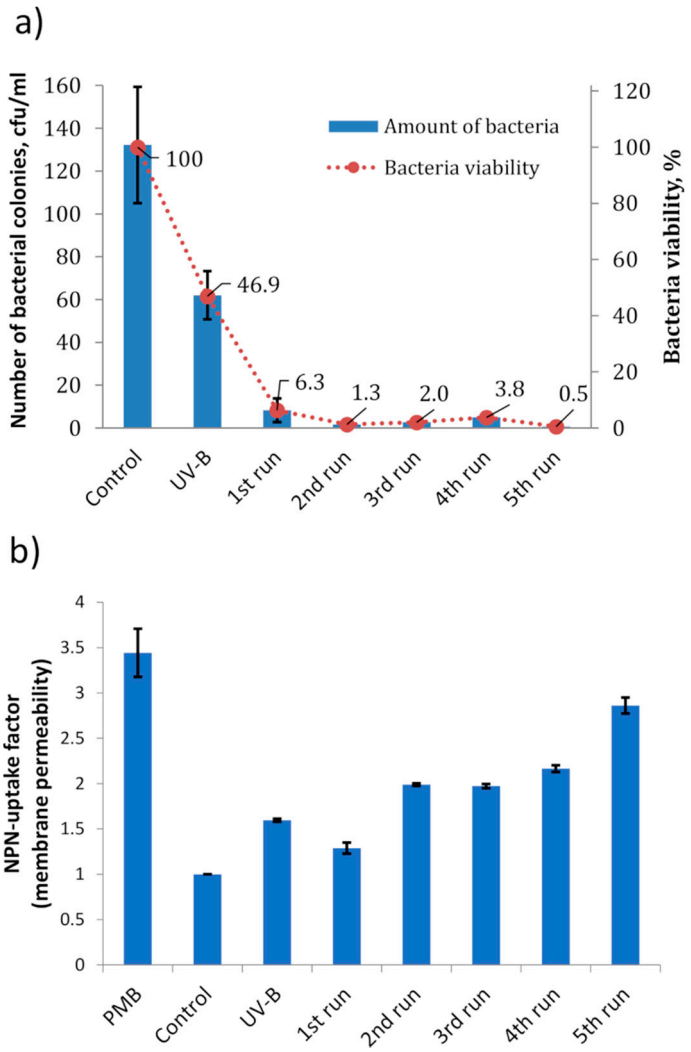

Figure 6. Results of *Salmonella typhimurium* SL1344 bacterial inactivation experiment using HDPE + TiO_2 under UV-B irradiation: (**a**) bacterial viability results of cycling test; (**b**) NPN uptake factor (membrane permeability results) during each run. The experiments were performed at 37 °C, the initial number of bacteria was 3×10^8 cfu/mL, dilution factor of 50,000.

To determine the effect of UV light on irradiated HDPE granules coated by TiO_2, firstly, the bactericidal effect induced by the light source was investigated. The obtained results showed that the viability of *Salmonella typhimurium* decreases 50% and the permeability of the outer membrane increases by half a unit. To reach the maximal permeability of the outer membrane (100%), we used 50 µg/mL of polymyxin B (PMB). This compound is an antibiotic which permeabilizes the outer membrane of Gram-negative bacteria and

depolarizes the cytoplasmic membrane when used at high concentrations [42]. Our investigation shows that the maximal NPN uptake factor in S. Typhimurium cells is about 3.5 with our experimental conditions. In order to determine if the efficiency of granules coated by TiO_2 decreases, we carried out five experiments in a row. The viability test showed that the addition of granules coated by TiO_2 strongly increased the bactericidal effect on S. Typhimurium cells. Only 6% of colonies were formed after the first experiment. The viability of bacteria was only about 1% after the next four experiments. An NPN uptake assay showed similar results. The first experiment with irradiated granules showed the weakest effect. The membrane permeability increased only 0.25 units compared to control. Interestingly, this is 0.25 units lower than in cells which were irradiated only by the UV light source. From the second to fourth experiment, NPN uptake was rather similar—two times higher than in the control sample. Permeability of the outer membrane was the highest after the last treatment. The NPN cell uptake factor was about 3.

TiO_2 generates short-lived singlet oxygen in an aerobic environment which has high efficiency in catalytic systems [43]. Our studies on the degradation of methylene blue solution are in agreement with that statement. The fading time of the solution was the shortest during the first experiment. Meanwhile, the viability of bacteria was not significantly affected by short-lived radicals due to slow diffusion into cells [44]. It has been found that titanium dioxide binds oxygen radicals on its surface, thus stabilizing them to long-lived radicals, and this is surface area dependent [43]. Long-lived superoxide and H_2O_2 radicals cause local damage to bacterial membranes [2]. It is very significant that the photocatalytic efficiency of titanium dioxide highly depends on the photosensitive surface and not just on a large amount of powder because a large amount of powder causes a screening effect [45]. Our investigation showed that a photosensitive active surface on granules increased with every series of our experiment.

Ruptures in cell membranes occur after treatment with nano-TiO_2 [46,47]. After damage to the cytoplasmic membrane, electron transport along the respiratory chain is impaired and therefore generation of intracellular ROS occurs [47]. Our previous study showed the formation of intracellular ROS and changes in the outer membrane when bacteria were irradiated with titanium oxide granules under UV-B light [28]. Thus, we can state that with the presented UV-B control results, we indicate the effect of irradiation, which causes damage to the bacterial envelope and DNA, after which bacteria are not able to multiply. In the samples with TiO_2-coated granules, we observed a cumulative effect of mechanical damage by TiO_2 to the outer bacterial membrane and the effect of stabilized ROS which caused the growth of intracellular ROS levels, followed by cell death. The granules we used stabilize the short-lived ROS in the medium, thus improving the bactericidal effect. In the following series, the amount of stabilized oxygen radicals was larger due to the increased photosensitive surface of titanium dioxide. Therefore, the bactericidal effect was enhanced.

3. Methodology

3.1. TiO_2 Synthesis

Anatase (TiO_2) films were deposited on the surface of HDPE beads (nominal size 2–4 mm, density 0.95 g/cm^3, obtained from GoodFellow, Huntingdon, UK) using magnetron sputtering with a physical vapor deposition system. A vacuum system including rotary and diffusion pumps enabled a base pressure of 2 mTorr. A circular Ti target (95 mm diameter, 99.99% purity) was used as a primary material for the sputtering process. Reactive magnetron sputtering was performed for 16 h at 300 W (0.8 A) power maintained by a pulsed DC power source, while the distance between magnetron and HDPE beads was 10 cm. TiO_2 deposition was carried out at 60 mTorr pressure using an Ar (5%)–O_2 gas mixture. After 8 h of magnetron sputtering, HDPE beads were flipped over to deposit TiO_2 on the other side. The thickness of the deposited film was approximately 100 nm. The thickness was measured indirectly. TiO_2 film was deposited on a flat quartz substrate under the

same parameters and thickness measurements of as-deposited TiO_2 films were performed using a stylus profiler (Ambios XP-200, Ambios Technology, Santa Cruz, CA, USA).

3.2. Photocatalysis and Bacterial Inactivation

The photocatalytic activity of the deposited TiO_2 films on HDPE beads was estimated by measuring photodegradation of methylene blue aqueous solution (MB, 10 mg/L) under UV-B irradiation produced by a medical lamp (PL-S 9W/01/2p 1CT, Philips, Amsterdam, The Netherlands) with an aluminum light reflector. Prior to each experiment, 1g of HDPE beads with TiO_2 film were immersed in a Petri dish filled with 10 mL of MB solution and kept in the dark for 1 h. Then, the sample was placed 10 cm below the lamp, and irradiation intensity measured at the sample level was around 5 mW/cm^2 (Thorlabs PM16-401 power meter was used, Dachau, Germany). During the photodegradation of MB experiments, the top of the glass container was covered by a highly transparent 500 µm thick fused silica disc in order to minimize the evaporation of MB solution. During the test, MB solution with samples was continuously mixed by a magnetic stirrer at 500 rpm and a constant temperature (21 °C) of MB solution was maintained using a Peltier module. The rate of degradation of MB was determined by a UV–Vis spectrophotometer (Jasco V-650, Tokyo, Japan) using absorbance at 664 nm. Measurements were repeated at 30 min intervals using 1 mL volume cuvettes and after that the MB solution was syringed back to the glass container with samples immediately.

3.2.1. Bacterial Cultivation

Gram-negative *Salmonella enterica* ser. *Typhimurium* SL1344, were cultivated as described in our previous publication [48] with some modifications: after incubation, an overnight culture was diluted with fresh LB medium to an optical density (OD_{600}) of 0.15 and grown in 50 mL LB medium with shaking at 220 rpm until the OD_{600} was 0.8–1.0. The cell preparation was then the same.

3.2.2. Bacterial Inactivation Test

The experiments were performed in a thermostatted vessel at 37 °C in which 3×10^8 cfu/mL (OD_{600} of 1) of *Salmonella typhimurium* cells were added to 10 mL of PBS buffer (pH 7.4) containing 0.1% glucose and 1 g of HDPE beads coated by TiO_2. The duration of treatment by a UV-B lamp (5 mW/cm^2) (PL-S 9W/01/2p 1CT, Philips, Amsterdam, Netherlands) was 60 min. The distance from the light source to the sample was 6 cm. Control samples were without granules and irradiation.

The viability of *Salmonella typhimurium* was determined by the spread plate method. After of incubation, 100 µL of each sample was taken from the vessel, diluted 50,000 times and plated on LB agar. Plates were incubated for 20–22 h at 37 °C and after incubation formed colonies were counted. The remaining suspension was centrifuged at 3000× *g* for 5 min at 4 °C (Heraeus ™ Megafuge ™ 16R, Thermo Scientific, Bremen, Germany). The pellet was collected with PBS buffer, pH 7.4, to obtain 3×10^8 cfu/mL (OD_{600} of 1) and further used for an NPN uptake factor assay for membrane permeability determination.

3.2.3. NPN Uptake Assay

N-phenyl-1-naphthylamine (NPN) is a hydrophobic fluorescent probe. The fluorescence of 1-NPN increases in a hydrophobic environment (e.g., membrane lipid bilayer). Due to this property, it is an appropriate dye for the determination of bacterial outer membrane permeability. After the irradiation with HDPE beads coated by TiO_2, samples of prepared bacterial suspensions (as described above) were mixed and placed in black 96-well plates at 100 µL per well by adding 10 µM of NPN. NPN fluorescence intensity was immediately measured in a TECAN GENios Pro™ (Tecan, Männedorf, Switzeland) plate reader at excitation wavelength of 350 nm and emission wavelength of 460 nm. The 1-NPN cell uptake factor is a ratio between the intensity of fluorescence values of the irradiated

bacterial suspension and a control sample. To reach the maximal uptake of NPN, we used 50 μg/mL of polymyxin B in a well with cells from a control cuvette.

3.3. Characterization

The surface morphology of deposited TiO_2 films on HDPE substrates was measured by scanning electron microscope (SEM, Hitachi S-3400 N, Tokyo, Japan). The analysis of elemental composition and elemental mapping was performed by energy dispersive X-ray spectroscopy (EDS, Bruker Quad 5040, Hamburg, Germany). An X-ray diffractometer operating with Cu Kα radiation (XRD, Bruker D8, Hamburg, Germany) was used to determine the crystal structure of synthesized TiO_2 films. Crystallite size was calculated by Topas software using Lorentzian deconvolution. An X-ray photoelectron spectroscope (XPS, PHI 5000 Versaprobe, Boston, MA, USA) was employed for the evaluation of chemical bonds and surface elemental composition. Monochromated 1486.6 eV Al radiation, 12.5 W beam power, 50 μm beam size and 45° were used in the XPS analysis.

4. Conclusions

In this paper, HDPE beads were used as floating substrates for TiO_2 film deposited by magnetron sputtering. Thin TiO_2 films with a thickness of 100 nm acted as photocatalyst material. XRD analysis confirmed that a nanocrystalline anatase structure was synthesized while SEM mapping views showed that even after cycling experiments, Ti and O were quite uniformly distributed over the whole area of the HDPE substrate. XPS data were in good agreement with experiments, showing additional elements after MB decomposition and bacterial inactivation as well as formation of polar molecule groups. During the photocatalytic cycling experiment, HDPE beads with TiO_2 film showed the highest photocatalytic activity for degradation of MB after the first run, where the absorbance at 664 nm decreased from 1.35 to 0.11 after 180 min of UV-B irradiation. However, with an increasing number of runs, the MB degradation rate decreased from 10.8×10^{-3} min^{-1} to 2.7×10^{-3} min^{-1}.

Meanwhile, bacterial inactivation results showed that the efficiency of granules coated by TiO_2 increased with every additional experiment, which was additionally confirmed by XPS (lower surface adsorption). The viability test showed no marked differences between experiments 2–5 but NPN uptake in cells showed increasing permeability of the outer membrane. This could be due to the increased photosensitive area of TiO_2 granules with each additional experiment. ROS stabilization in medium is more effective with increasing TiO_2 surface area [43]. Additionally, it is known that small TiO_2 nanoparticles cause damage to the lipid bilayer and membrane potential is lost [46]. In our experiments, we combined TiO_2, stabilized ROS and the intracellular ROS bactericidal effect with S. Typhimurium cells.

Author Contributions: Conceptualization and supervision, M.L.; methodology, S.V. and M.U.; investigation, S.T., S.V., M.U., S.S. and E.D.; writing—original draft preparation, S.V., M.U. and S.S.; writing—review and editing, S.V., M.U., S.S. and M.L.; visualization, S.T., M.U. and S.V. All authors have read and agreed to the published version of the manuscript.

Funding: This research is funded by the European Social Fund according to the activity "Improvement of researchers" qualification by implementing world-class R&D projects of Measure No. 09.3.3-LMT-K-712, project "Investigation of the application of TiO2 and ZnO for the visible light assisted photocatalytical disinfection of the biologically contaminated water" (09.3.3-LMT-K-712-01-0175).

Data Availability Statement: Not applicable.

Acknowledgments: The authors express gratitude to Darius Milcius and Albinas Svirskis for their input in material synthesis; Rimantas Daugelavicius and Neringa Kuliesiene for their input in data analysis and interpretation; Mindaugas Aikas, Rolandas Uscila and Deimante Vasiliauske for their valuable input in preparation and conduction of photocatalysis-based experiments.

Conflicts of Interest: The authors declare no conflict of interest.

References

1. Védrine, J.C. Importance, features and uses of metal oxide catalysts in heterogeneous catalysis. *Chin. J. Catal.* **2019**, *40*, 1627–1636. [CrossRef]
2. Anastas, P.T.; Bartlett, L.B.; Kirchhoff, M.M.; Williamson, T.C. The role of catalysis in the design, development, and implementation of green chemistry. *Catal. Today* **2000**, *55*, 11–22. [CrossRef]
3. Courty, P.R.; Chauvel, A. Catalysis, the turntable for a clean future. *Catal. Today* **1996**, *29*, 3–15. [CrossRef]
4. Russell, H.S.; Frederickson, L.B.; Hertel, O.; Ellermann, T.; Jensen, S.S. A Review of Photocatalytic Materials for Urban NOx Remediation. *Catalysts* **2021**, *11*, 695. [CrossRef]
5. Kutuzova, A.; Dontsova, T.; Kwapinski, W. Application of TiO2-Based Photocatalysts to Antibiotics Degradation: Cases of Sulfamethoxazole, Trimethoprim and Ciprofloxacin. *Catalysts* **2021**, *11*, 728. [CrossRef]
6. Sirivallop, A.; Escobedo, S.; Areerob, T.; de Lasa, H.; Chiarakorn, S. Photocatalytic Conversion of Organic Pollutants in Air: Quantum Yields Using a Silver/Nitrogen/TiO2 Mesoporous Semiconductor under Visible Light. *Catalysts* **2021**, *11*, 529. [CrossRef]
7. Anastas, P.T.; Kirchhoff, M.M.; Williamson, T.C. Catalysis as a foundational pillar of green chemistry. *Appl. Catal. A Gen.* **2001**, *221*, 3–13. [CrossRef]
8. Bover-Cid, S.; Belletti, N.; Aymerich, T.; Garriga, M. Modelling the impact of water activity and fat content of dry-cured ham on the reduction of Salmonella enterica by high pressure processing. *Meat Sci.* **2017**, *123*, 120–125. [CrossRef]
9. Pino-Sandoval, D.; Villanueva-Rodríguez, M.; Cantú-Cárdenas, M.E.; Hernández-Ramírez, A. Performance of Ag-Cu/TiO2 photocatalyst prepared by sol-gel method on the inactivation of Escherichia coli and Salmonella typhimurium. *J. Environ. Chem. Eng.* **2020**, *8*, 104539. [CrossRef]
10. Zhang, C.; Xu, L.; Mou, X.; Xu, H.; Liu, J.; Miao, Y.; Wang, X.C.; Li, X. Characterization and evolution of antibiotic resistance of Salmonella in municipal wastewater treatment plants. *J. Environ. Manag.* **2019**, *251*, 109547. [CrossRef] [PubMed]
11. Lin, Y.w.; Li, D.; Gu, A.Z.; Zeng, S.y.; He, M. Bacterial regrowth in water reclamation and distribution systems revealed by viable bacterial detection assays. *Chemosphere* **2016**, *144*, 2165–2174. [CrossRef] [PubMed]
12. Dolejska, M.; Frolkova, P.; Florek, M.; Jamborova, I.; Purgertova, M.; Kutilova, I.; Cizek, A.; Guenther, S.; Literak, I. CTX-M-15-producing Escherichia coli clone B2-O25b-ST131 and Klebsiella spp. isolates in municipal wastewater treatment plant effluents. *J. Antimicrob. Chemother.* **2011**, *66*, 2784–2790. [CrossRef] [PubMed]
13. Huang, J.J.; Hu, H.Y.; Lu, S.Q.; Li, Y.; Tang, F.; Lu, Y.; Wei, B. Monitoring and evaluation of antibiotic-resistant bacteria at a municipal wastewater treatment plant in China. *Environ. Int.* **2012**, *42*, 31–36. [CrossRef] [PubMed]
14. Fan, X.; Song, Y. Advanced Oxidation Process as a Postharvest Decontamination Technology To Improve Microbial Safety of Fresh Produce. *J. Agric. Food Chem.* **2020**, *68*, 12916–12926. [CrossRef] [PubMed]
15. Bounty, S.; Rodriguez, R.A.; Linden, K.G. Inactivation of adenovirus using low-dose UV/H2O2 advanced oxidation. *Water Res.* **2012**, *46*, 6273–6278. [CrossRef]
16. del Álamo, A.C.; Pariente, M.I.; Vasiliadou, I.; Padrino, B.; Puyol, D.; Molina, R.; Martínez, F. Removal of pharmaceutical compounds from urban wastewater by an advanced bio-oxidation process based on fungi Trametes versicolor immobilized in a continuous RBC system. *Environ. Sci. Pollut. Res.* **2018**, *25*, 34884–34892. [CrossRef]
17. Wang, B.; Song, Z.; Sun, L. A review: Comparison of multi-air-pollutant removal by advanced oxidation processes—Industrial implementation for catalytic oxidation processes. *Chem. Eng. J.* **2021**, *409*, 128136. [CrossRef]
18. Liu, L.; Chen, Z.; Zhang, J.; Shan, D.; Wu, Y.; Bai, L.; Wang, B. Treatment of industrial dye wastewater and pharmaceutical residue wastewater by advanced oxidation processes and its combination with nanocatalysts: A review. *J. Water Process Eng.* **2021**, *42*, 102122. [CrossRef]
19. Kanakaraju, D.; Glass, B.D.; Oelgemöller, M. Advanced oxidation process-mediated removal of pharmaceuticals from water: A review. *J. Environ. Manag.* **2018**, *219*, 189–207. [CrossRef]
20. Chen, Y.; Duan, X.; Zhou, X.; Wang, R.; Wang, S.; Ren, N.; Ho, S.-H. Advanced oxidation processes for water disinfection: Features, mechanisms and prospects. *Chem. Eng. J.* **2021**, *409*, 128207. [CrossRef]
21. Russo, M.; Iervolino, G.; Vaiano, V. W-Doped ZnO Photocatalyst for the Degradation of Glyphosate in Aqueous Solution. *Catalysts* **2021**, *11*, 234. [CrossRef]
22. Xing, Z.; Zhang, J.; Cui, J.; Yin, J.; Zhao, T.; Kuang, J.; Xiu, Z.; Wan, N.; Zhou, W. Recent advances in floating TiO2-based photocatalysts for environmental application. *Appl. Catal. B Environ.* **2018**, *225*, 452–467. [CrossRef]
23. Nasir, A.M.; Jaafar, J.; Aziz, F.; Yusof, N.; Salleh, W.N.W.; Ismail, A.F.; Aziz, M. A review on floating nanocomposite photocatalyst: Fabrication and applications for wastewater treatment. *J. Water Process Eng.* **2020**, *36*, 101300. [CrossRef]
24. Faramarzpour, M.; Vossoughi, M.; Borghei, M. Photocatalytic degradation of furfural by titania nanoparticles in a floating-bed photoreactor. *Chem. Eng. J.* **2009**, *146*, 79–85. [CrossRef]
25. Xue, H.; Jiang, Y.; Yuan, K.; Yang, T.; Hou, J.; Cao, C.; Feng, K.; Wang, X. Floating photocatalyst of B-N-TiO 2 /expanded perlite: A sol-gel synthesis with optimized mesoporous and high photocatalytic activity. *Sci. Rep.* **2016**, *6*, 2–10. [CrossRef] [PubMed]
26. Das, S.; Mahalingam, H. Reusable floating polymer nanocomposite photocatalyst for the efficient treatment of dye wastewaters under scaled-up conditions in batch and recirculation modes. *J. Chem. Technol. Biotechnol.* **2019**, *94*, 2597–2608. [CrossRef]
27. Valdez-Castillo, M.; Saucedo-Lucero, J.O.; Arriaga, S. Photocatalytic inactivation of airborne microorganisms in continuous flow using perlite-supported ZnO and TiO2. *Chem. Eng. J.* **2019**, *374*, 914–923. [CrossRef]

28. Varnagiris, S.; Urbonavicius, M.; Sakalauskaite, S.; Daugelavicius, R.; Pranevicius, L.; Lelis, M.; Milcius, D. Floating TiO2 photocatalyst for efficient inactivation of E. coli and decomposition of methylene blue solution. *Sci. Total Environ.* **2020**, *720*, 137600. [CrossRef]
29. Sboui, M.; Lachheb, H.; Bouattour, S.; Gruttadauria, M.; La Parola, V.; Liotta, L.F.; Boufi, S. TiO2/Ag2O immobilized on cellulose paper: A new floating system for enhanced photocatalytic and antibacterial activities. *Environ. Res.* **2021**, *198*, 111257. [CrossRef]
30. Wang, B.; Wei, S.; Guo, L.; Wang, Y.; Liang, Y.; Xu, B.; Pan, F.; Tang, A.; Chen, X. Effect of deposition parameters on properties of TiO2 films deposited by reactive magnetron sputtering. *Ceram. Int.* **2017**, *43*, 10991–10998. [CrossRef]
31. Lee, M.K.; Park, Y.C. Super-hydrophilic anatase TiO2thin film in-situ deposited by DC magnetron sputtering. *Thin Solid Films* **2017**, *638*, 9–16. [CrossRef]
32. Singh, P.; Kaur, D. Room temperature growth of nanocrystalline anatase TiO2thin films by dc magnetron sputtering. *Phys. B Condens. Matter* **2010**, *405*, 1258–1266. [CrossRef]
33. Awaja, F.; Gilbert, M.; Kelly, G.; Fox, B.; Pigram, P.J. Adhesion of polymers. *Prog. Polym. Sci.* **2009**, *34*, 948–968. [CrossRef]
34. Popelka, A.; Novák, I.; Al-Maadeed, M.A.S.A.; Ouederni, M.; Krupa, I. Effect of corona treatment on adhesion enhancement of LLDPE. *Surf. Coat. Technol.* **2018**, *335*, 118–125. [CrossRef]
35. Tendero, C.; Tixier, C.; Tristant, P.; Desmaison, J.; Leprince, P. Atmospheric pressure plasmas: A review. *Spectrochim. Acta Part B At. Spectrosc.* **2006**, *61*, 2–30. [CrossRef]
36. Dixon, D.; Meenan, B.J. Atmospheric dielectric barrier discharge treatments of polyethylene, polypropylene, polystyrene and poly(ethylene terephthalate) for enhanced adhesion. *J. Adhes. Sci. Technol.* **2012**, *26*, 2325–2337. [CrossRef]
37. Communication, S.; Engineering, C. Surface modification of polypropylene in an impulse corona discharge. *Korean J. Chem. Eng.* **1996**, *13*, 97–100.
38. Stewart, R.; Goodship, V.; Guild, F.; Green, M.; Farrow, J. Investigation and demonstration of the durability of air plasma pre-treatment on polypropylene automotive bumpers. *Int. J. Adhes. Adhes.* **2005**, *25*, 93–99. [CrossRef]
39. Kozak, M.; Cirik, K.; Başak, S. Treatment of textile wastewater using combined anaerobic moving bed biofilm reactor and powdered activated carbon-aerobic membrane reactor. *J. Environ. Chem. Eng.* **2021**, *9*, 105596. [CrossRef]
40. Fanta, A.B.; Nair, A.M.; Sægrov, S.; Østerhus, S.W. Phosphorus removal from industrial discharge impacted municipal wastewater using sequencing batch moving bed biofilm reactor. *J. Water Process Eng.* **2021**, *41*, 102034. [CrossRef]
41. Shitu, A.; Liu, G.; Zhang, Y.; Ye, Z.; Zhao, J.; Zhu, S.; Liu, D. Enhancement of mariculture wastewater treatment using moving bed biofilm reactors filled with modified biocarriers: Characterisation, process performance and microbial community evaluation. *J. Environ. Manag.* **2021**, *291*, 112724. [CrossRef] [PubMed]
42. Daugelavicius, R.; Bakiene, E.; Bamford, D.H. Stages of polymyxin B interaction with the Escherichia coli cell envelope. *Antimicrob. Agents Chemother.* **2000**, *44*, 2969–2978. [CrossRef] [PubMed]
43. Wang, D.; Zhao, L.; Wang, D.; Yan, L.; Jing, C.; Zhang, H.; Guo, L.H.; Tang, N. Direct evidence for surface long-lived superoxide radicals photo-generated in TiO2 and other metal oxide suspensions. *Phys. Chem. Chem. Phys.* **2018**, *20*, 18978–18985. [CrossRef] [PubMed]
44. Giannakis, S.; Polo López, M.I.; Spuhler, D.; Sánchez Pérez, J.A.; Fernández Ibáñez, P.; Pulgarin, C. Solar disinfection is an augmentable, in situ-generated photo-Fenton reaction—Part 1: A review of the mechanisms and the fundamental aspects of the process. *Appl. Catal. B Environ.* **2016**, *199*, 199–223. [CrossRef]
45. Carré, G.; Hamon, E.; Ennahar, S.; Estner, M.; Lett, M.C.; Horvatovich, P.; Gies, J.P.; Keller, V.; Keller, N.; Andre, P. TiO2 photocatalysis damages lipids and proteins in Escherichia coli. *Appl. Environ. Microbiol.* **2014**, *80*, 2573–2581. [CrossRef]
46. Khater, M.S.; Kulkarni, G.R.; Khater, S.S.; Gholap, H.; Patil, R. Study to elucidate effect of titanium dioxide nanoparticles on bacterial membrane potential and membrane permeability. *Mater. Res. Express* **2020**, *7*, 035005. [CrossRef]
47. Ranjan, S.; Ramalingam, C. Titanium dioxide nanoparticles induce bacterial membrane rupture by reactive oxygen species generation. *Environ. Chem. Lett.* **2016**, *14*, 487–494. [CrossRef]
48. Kuliesiene, N.; Sakalauskaite, S.; Tuckute, S.; Urbonavicius, M.; Varnagiris, S.; Daugelavicius, R.; Lelis, M. TiO2Application for the Photocatalytical Inactivation of S. enterica, E. coli and M. luteus Bacteria Mixtures. *Environ. Clim. Technol.* **2020**, *24*, 418–429. [CrossRef]